Int. J. Heat Mass Transfer. Vol. 31, No. 4, pp. 875–890, 1988
Printed in Great Britain

0017–9310/88 $3.00 + 0.00

Thermophoresis of aerosol particles in laminar flow over inclined plates

VIJAY K. GARG†
Department of Mechanical Engineering, Ohio State University, Columbus, OH 43210-1107, U.S.A.

and

S. JAYARAJ
Department of Mechanical Engineering, Regional Engineering College, Calicut 673601, India

(*Received* 22 *December* 1986 *and in final form* 15 *September* 1987)

Abstract—We analyze numerically the thermophoretic deposition of small particles due to the impingement of a laminar slot jet on an inclined plate. The governing boundary layer type equations are solved by an implicit finite difference technique using grid adaptation for the cold, hot and adiabatic plate conditions. The particle concentration at the cold plate is found to be almost independent of the location along the plate, and of the angle of inclination of the plate as long as the plate temperature (less than the free stream temperature) and thermophoretic coefficient are constant. Adjacent to the hot plate is a critical layer the thickness of which depends upon both the location along the plate and the angle of inclination. Whether this layer is free or full of particles depends upon the product of Prandtl number and thermophoretic coefficient being less than or greater than unity. Results for the adiabatic plate are very similar to those for the hot plate except that the particle concentration gradient is zero at the plate. The dissipation of mechanical energy also has a significant effect on the particle concentration.

1. INTRODUCTION

THERMOPHORESIS is a phenomenon by which submicrometer sized particles suspended in a non-isothermal gas acquire a mean speed relative to the gas in the direction of decreasing temperature. The thermophoretic force experienced by small particles is caused by the differential molecular bombardment giving rise to radiometric forces [1]. This phenomenon is of considerable importance for particles having radii as large as 10 μm in fields with temperature gradients of the order of 5 K mm^{-1}. Some of the applications of thermophoresis are in removing small particles from gas streams, in determining exhaust gas particle trajectories from combustion devices, in studying the particulate material deposition on turbine blades, etc. [2]. It has also been demonstrated recently that thermophoresis is the dominant mass transfer mechanism in the modified chemical vapor deposition (MCVD) process used in the fabrication of optical fiber performs [3]. This subject is also important in view of its relevance to postulated accidents by radioactive particle deposition in nuclear reactors. The fact that scrubbing is more effective when the dusty air is preheated has been ascribed to thermophoresis. The reverse effect of thermophoresis, namely, the repulsion of particles from a hot wall and the formation of a particle-free layer around hot objects, has also been observed.

Despite the practical importance of thermophoresis, there have been only limited reports regarding the calculation of particle concentration in a flow field. Studies by Derjaguin *et al.* [4, 5] were in connection with simple channel flow for the measurement of thermophoretic velocity. Goren [6] gives a detailed analysis of thermophoresis over a flat plate. The laminar tube flow solution for thermophoretic deposition of small particles was reported by Walker *et al.* [7]. A recent paper by Epstein *et al.* [8] deals with thermophoretic deposition in natural convection flow from a vertical plate. This analysis is only for the cold surface but both laminar and turbulent flow conditions are considered. The external transverse flow situation past a circular cylinder was analyzed by Homsy *et al.* [9] with the help of the Blasius series. Apart from these, there are reports regarding the laser modification of thermophoretic deposition in tube flow applied to the MCVD process used in the manufacture of graded index optical fiber performs [10–12].

The present work involves the thermophoresis of aerosol particles in the laminar incompressible boundary layer over inclined plates (Fig. 1). The study includes cold, hot and adiabatic wall conditions for the plate. The hydrodynamic and thermal boundary layers are computed before solving for the concentration boundary layer. The pressure gradient

† On sabbatical leave from Indian Institute of Technology, Kanpur, India.

NOMENCLATURE

Lower case symbols in parentheses are the dimensional counterparts of the dimensionless quantities denoted by upper case symbols on the same line.

$C, (c)$	particle concentration per unit volume of gas
C_p	specific heat at constant pressure
Ec	Eckert number, $u_\infty^2/C_p t_\infty$
h	local heat transfer coefficient
J	local dimensionless flux of particles at the plate
K	thermophoretic coefficient
L	thickness of slot jet impinging on the plate
Nu	local Nusselt number
$P, (p)$	pressure
Pr	Prandtl number
Re	Reynolds number, $u_\infty L/v$
$T, (t)$	temperature
$U, V, (u, v)$	velocity components in (x, y) directions, respectively
U_s	dimensionless potential flow velocity at the plate
$\mathbf{v}_t$	thermophoretic velocity vector
$V_T, (v_t)$	thermophoretic velocity component normal to the plate
$X, Y, (x, y)$	coordinates along and normal to the plate, respectively
$\Delta X, \Delta Y$	mesh sizes in X, Y directions, respectively
Y_c	critical layer thickness [dimensionless].

Greek symbols

β	angle of inclination of the plate
δ_c	concentration boundary layer thickness
θ	dimensionless temperature defined by $(T-1)/(T_w-1)$
ν	kinematic viscosity of the fluid
ρ	density of the fluid
ψ	stream function.

Subscripts

j, k	location in X, Y directions, respectively
w	value at the plate surface
∞	value in the free stream.

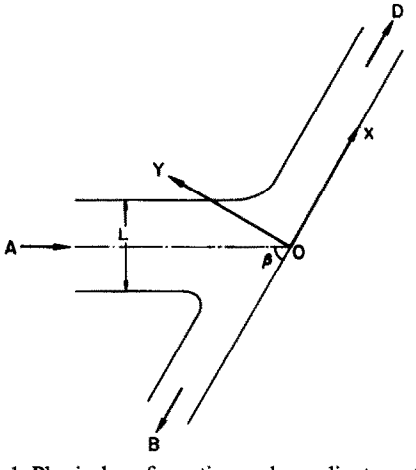

FIG. 1. Physical configuration and coordinate system.

required for the solution of the momentum equation is computed by considering the direct impingement of two unequal inviscid jets. The concentration boundary layer results are presented for a wide range of parameters. However, the Prandtl number is kept constant (0.7) throughout the study. Also constant thermophysical properties are assumed.

2. GOVERNING EQUATIONS

Consider a gaseous slot jet containing suspended aerosol particles impinging on a plate at an angle β as shown in Fig. 1. The particle concentration is assumed to be dilute enough for the velocity and temperature profiles to pertain to those for a particle-free gas. For particles of unit density and 1 μm radius, this assumption limits the analysis to aerosol concentrations less than about 10^7 particles per cubic centimeter of the gas at normal temperature and pressure [6]. This is indeed the case for most thermophoretic applications. The velocity and temperature distributions in the laminar flow region over the plate are therefore governed by the usual boundary layer equations.

For a steady, laminar, two-dimensional, incompressible flow with constant properties, these equations in dimensionless form are [13]

$$\frac{\partial U}{\partial X} + \frac{\partial V}{\partial Y} = 0 \tag{1}$$

$$U\frac{\partial U}{\partial X} + V\frac{\partial U}{\partial Y} = \frac{\partial^2 U}{\partial Y^2} - \frac{dP}{dX} \tag{2}$$

$$U\frac{\partial T}{\partial X} + V\frac{\partial T}{\partial Y} = \frac{1}{Pr}\frac{\partial^2 T}{\partial Y^2} + Ec\left(\frac{\partial U}{\partial Y}\right)^2 \tag{3}$$

where the dimensionless variables are defined as

$$X = x/L, \quad Y = Re^{1/2}y/L, \quad T = t/t_\infty,$$
$$U = u/u_\infty, \quad V = Re^{1/2}v/u_\infty, \quad P = (p-p_\infty)/(\rho u_\infty^2).$$

The boundary conditions are

$$U(X,0)=0,\quad V(X,0)=0,\quad U(X,\infty)=U_s(X),$$
$$T(X,\infty)=1,\quad U(0,Y)=U_s(0),\quad T(0,Y)=1 \quad (4)$$

and

$$T(X,0)=T_w \quad \text{for an isothermal wall}$$

or

$$\partial T(X,0)/\partial Y=0 \quad \text{for an adiabatic wall.}$$

It should be pointed out that the boundary layer equations are really not valid at $X=0$. However, for the solution of equations (1)–(3) one boundary condition on U and T in the X-direction is required. The pressure gradient required in equation (2) is obtained by solving the governing equations for the direct impact of two unequal, inviscid jets. The detailed numerical solution of equations (1)–(3) is presented elsewhere [14] for isothermal plate conditions.

The temperature gradient established in the thermal boundary layer drives the particles either towards the plate where they get deposited or away from the plate thereby forming a critical layer adjacent to the plate. The velocity acquired by the small particles relative to the gas velocity, known as the thermophoretic velocity, is related to the temperature gradient in the flow field by

$$\mathbf{v}_t=-K(v/t)\nabla T. \quad (5)$$

The thermophoretic coefficient K depends mainly upon the Knudsen number. A number of formulations are available in the literature for the determination of K depending upon the regime of flow [4, 5, 15]. The semiempirical formula proposed by Talbot *et al.* [16] can be used for a wide range of Knudsen numbers. The value of K lies between 0.25 and 1.25 in most cases. For the present study K is considered as a parameter independent of temperature.

Some of the standard assumptions made for the simplification of the mass conservation equation for thermophoretic analysis are given below.

(1) Duc to the boundary layer behavior, the temperature gradient, $\partial t/\partial y$, is much larger than $\partial t/\partial x$. Also the gas velocity u is large compared to v. Since the thermophoretic velocity components are given by equation (5), it follows that the component normal to the plate, v_t, is the only one of importance. It is given by

$$v_t=-K(v/t)\partial t/\partial y. \quad (6)$$

(2) The particles are assumed to be sufficiently small so that the relaxation time scale for particle motion is several orders of magnitude smaller than that for the gas flow. This implies that in the absence of thermophoresis the particles move with the gas at the local gas velocity.

(3) For micrometer sized particles in air at normal temperature and pressure the Schmidt number is very large ($O(10^5)$). This implies that the Brownian diffusion sublayer is so thin, even on the boundary layer scale, that it does not alter the thermophoretic particle deposition rate. Hence the only effect of Brownian diffusion is to create an extremely thin particle concentration sublayer adjacent to the solid surface when the surface is colder than the surrounding gas and near a critical layer away from the surface when it is heated. Accordingly the Brownian diffusion is neglected.

(4) Thermal radiation is neglected.

With these assumptions and with the usual boundary layer approximations, the conservation law for particle concentration is

$$\partial(cu)/\partial x+\partial[c(v+v_t)]/\partial y=0. \quad (7)$$

Substitution of the continuity equation (1), and introduction of dimensionless variables reduces this equation to

$$U\frac{\partial C}{\partial X}+V\frac{\partial C}{\partial Y}+\frac{\partial}{\partial Y}(CV_T)=0 \quad (8)$$

where

$$V_T=Re^{1/2}v_t/u_\infty=-(K/T)\,\partial T/\partial Y$$

and

$$C=c/c_\infty.$$

The boundary conditions are

$$C(0,Y)=1 \quad \text{and} \quad C(X,\infty)=1. \quad (9)$$

In the absence of Brownian diffusion equation (8) is first order in Y, thus requiring only one boundary condition for C in the Y-direction. For a cold wall a non-zero particle concentration at $Y=0$ is determined by solving equations (8) and (9). Strictly speaking, this concentration is the one at the outer edge of the very thin Brownian sublayer which is considered of negligible thickness in our analysis. For a hot wall the particle concentration at $Y=0$ tends to ∞ for $PrK>1$, and to $-\infty$ for $PrK<1$ [6]. Though Goren's analysis [6] is for thermophoresis over a flat plate at zero incidence, a similar analysis carried out for thermophoresis over a wedge also reveals the presence of a critical layer close to the surfaces of the wedge. In our case, the plate held at right angles to the flow represents a wedge of angle 180°. It is therefore expected that a critical layer exists close to a hot plate held at any angle.

3. NUMERICAL SOLUTION

As mentioned previously, the detailed finite-difference solution of the hydrodynamic and thermal boundary layers (equations (1)–(3)) is available elsewhere [14]. The solution procedure for the concentration equation is explained here. A two-dimensional rectangular mesh is superimposed on the flow field. We use indices (j,k) to indicate the position of a point in the boundary layer. Let the plate surface be

represented by $k = 0$, the edge of the boundary layer by $k = n+1$, and the stagnation point by $j = 0$. Forward differences are used to find the dimensionless thermophoretic velocity component, V_T, from

$$V_{T_{j+1,k}} = -\frac{K}{\Delta Y}\frac{T_{j+1,k+1}-T_{j+1,k}}{T_{j+1,k}}. \quad (10)$$

In order to satisfy the sufficient conditions [17] for a meaningful solution of a tridiagonal or bidiagonal set of equations, four different discretization forms of equation (8) are used for the cold and hot plate surface conditions.

Cold plate ($V < 0$)

$$U_{j+1,k}\frac{C_{j+1,k}-C_{j,k}}{\Delta X} + V_{j+1,k}\frac{C_{j+1,k+1}-C_{j+1,k}}{\Delta Y} + \frac{C_{j+1,k+1}V_{T_{j+1,k+1}}-C_{j+1,k}V_{T_{j+1,k}}}{\Delta Y} = 0. \quad (11)$$

Cold plate ($V > 0$)

$$U_{j+1,k}\frac{C_{j+1,k}-C_{j,k}}{\Delta X} + V_{j+1,k}\frac{C_{j+1,k}-C_{j+1,k-1}}{\Delta Y} + \frac{C_{j+1,k+1}V_{T_{j+1,k+1}}-C_{j+1,k}V_{T_{j+1,k}}}{\Delta Y} = 0. \quad (12)$$

Hot plate ($V < 0$)

$$U_{j+1,k}\frac{C_{j+1,k}-C_{j,k}}{\Delta X} + V_{j+1,k}\frac{C_{j+1,k+1}-C_{j+1,k}}{\Delta Y} + \frac{C_{j+1,k}V_{T_{j+1,k}}-C_{j+1,k-1}V_{T_{j+1,k-1}}}{\Delta Y} = 0. \quad (13)$$

Hot plate ($V > 0$)

$$U_{j+1,k}\frac{C_{j+1,k}-C_{j,k}}{\Delta X} + V_{j+1,k}\frac{C_{j+1,k}-C_{j+1,k-1}}{\Delta Y} + \frac{C_{j+1,k}V_{T_{j+1,k}}-C_{j+1,k-1}V_{T_{j+1,k-1}}}{\Delta Y} = 0. \quad (14)$$

The above discretizations are first-order accurate in ΔY for V_T, and in ΔX and ΔY for C. The solution is carried out in a marching procedure starting from the stagnation point ($X = 0$) in either direction ($X > 0$ or $X < 0$). The velocity and temperature distributions are obtained at any X location ($j+1$) before solving equation (10) and an appropriate one amongst equations (11)–(14). For a cold plate, equation (11) or (12) written for $k = 0$ (1) n leads to either a bidiagonal or a tridiagonal set of $n+1$ linear equations that can be easily solved for the $n+1$ unknown values of C at the X-location ($j+1$). For a hot wall, a critical layer exists close to the wall in the absence of Brownian diffusion, as explained already. The presence of this critical layer necessitates a suitable boundary condition ($C = \pm\infty$) to be imposed at the wall. Hence in this case, C values are computed at n internal points along the Y-direction using equation (13) or (14).

Table 1. Step size in X-direction

$\lvert\Delta X\rvert$	Number of steps marched
10^{-5}	20
2×10^{-5}	10
5×10^{-5}	12
10^{-4}	10
2×10^{-4}	10
5×10^{-4}	12
10^{-3}	10
2×10^{-3}	10
5×10^{-3}	12
10^{-2}	90
2×10^{-2}	100

The computer programme takes care of the fact that the boundary layer thicknesses increase as we move away from the stagnation point. Thus we increase n as we march in the X-direction. The value of n is chosen so as to ensure that there are at least 3–4 points for $k \leqslant n$ for which $U \approx U_s$, $T \approx 1$, and $C \approx 1$. A variable grid size is used in the X-direction. Table 1 gives the values of ΔX used and the number of steps marched with each ΔX. Along the Y-direction a self-adaptive grid is used [18, 19]. For accurate results, this is essential specially for the hot wall condition in which the particle concentration approaches $\pm\infty$ as the wall is approached. This requires modifications to equation (10) for the k-value on either side of which ΔY is different, as described by Hornbeck [20]. The minimum value of ΔY was set at 0.005 and the maximum at 0.05. The self-adaptive grid generation technique distributes values of ΔY within this range. As many as 500 steps in the Y-direction were required for some values of angle β at the farthest downstream location $X = 3$.

4. RESULTS AND DISCUSSION

Typical results of the computations are shown in Figs. 2–20. The Prandtl number is kept constant at 0.7 throughout the study. The analysis is carried out for cold, hot and adiabatic plate conditions with different plate temperatures, amount of viscous dissipation and thermophoretic coefficient. The concentration profiles computed for the flat plate at zero incidence are found to be in excellent agreement with those of Goren [6].

4.1. *Flow characteristics*

Figure 2 shows the streamlines over a plate inclined at $\beta = 15°$. The values of dimensionless stream function ψ noted on the various curves in this figure were computed from

$$\psi = \int_0^Y U\,dY. \quad (15)$$

Similar streamlines were obtained for other inclinations of the plate, with the pattern becoming sym-

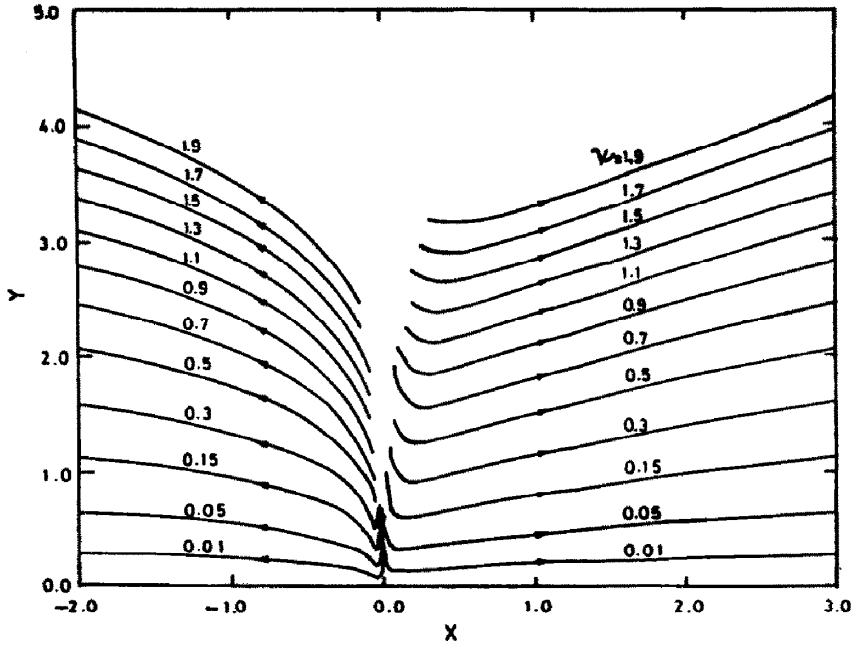

FIG. 2. Streamlines over an inclined plate for $\beta = 15°$.

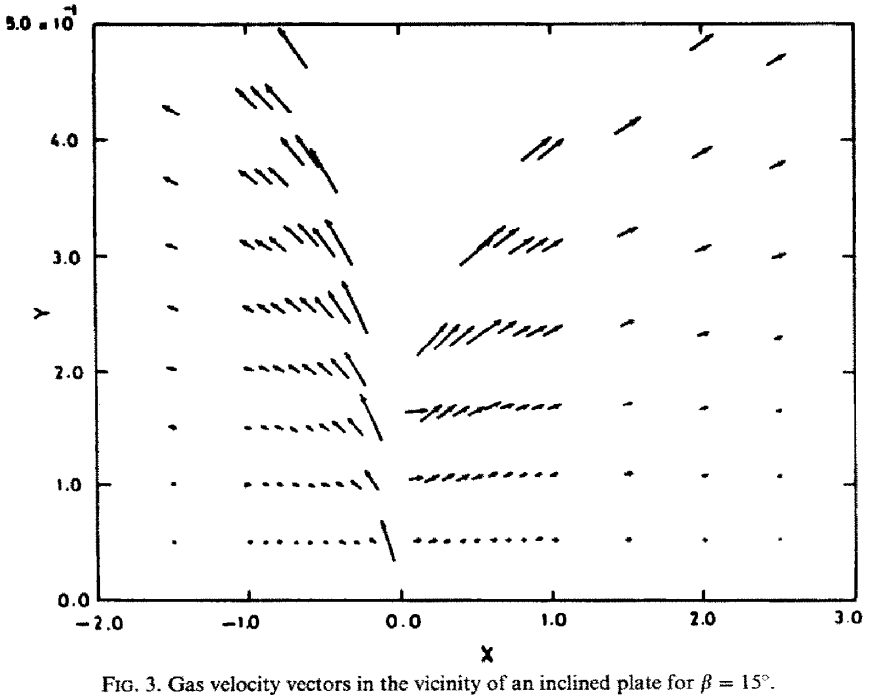

FIG. 3. Gas velocity vectors in the vicinity of an inclined plate for $\beta = 15°$.

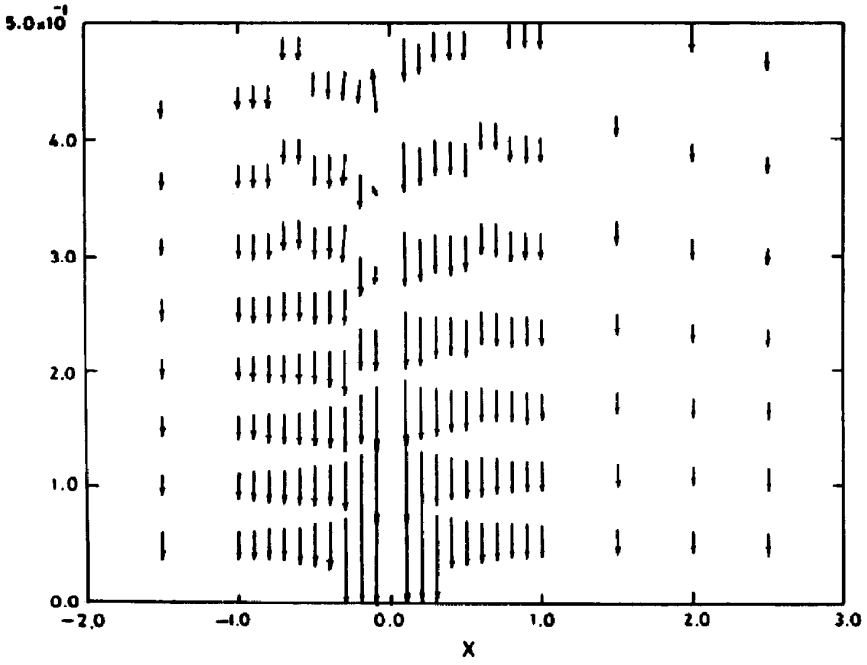

FIG. 4. Particle velocity vectors in the vicinity of a cold inclined plate for $\beta = 15°$ ($Pr = 0.7$, $Ec = 0$, $K = 0.75$, $T_w = 0.25$).

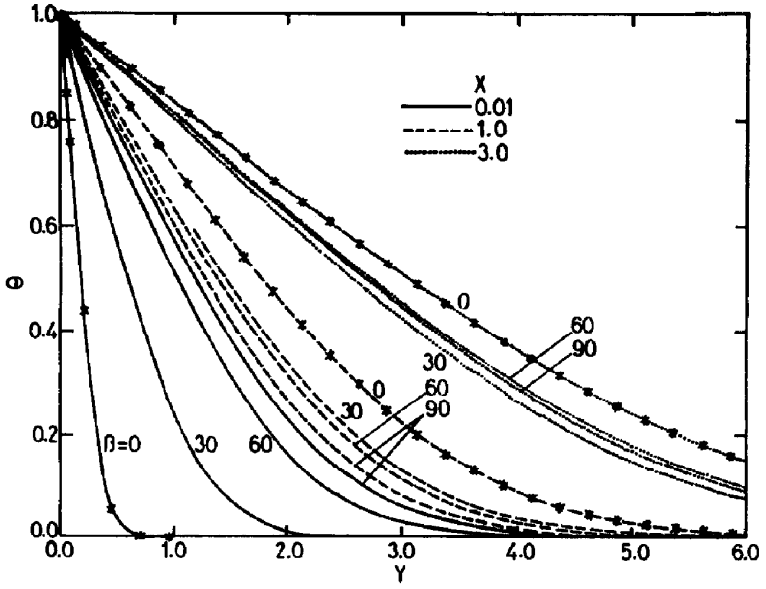

FIG. 5. Normalized temperature profiles over an isothermal plate ($Pr = 0.7$, $Ec = 0$).

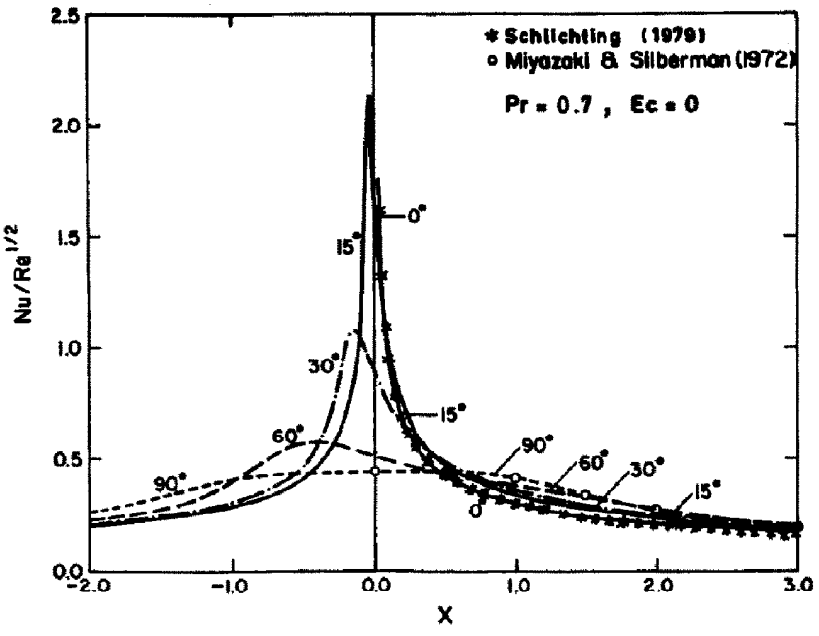

FIG. 6. Local Nusselt number over an isothermal plate ($Pr = 0.7$, $Ec = 0$).

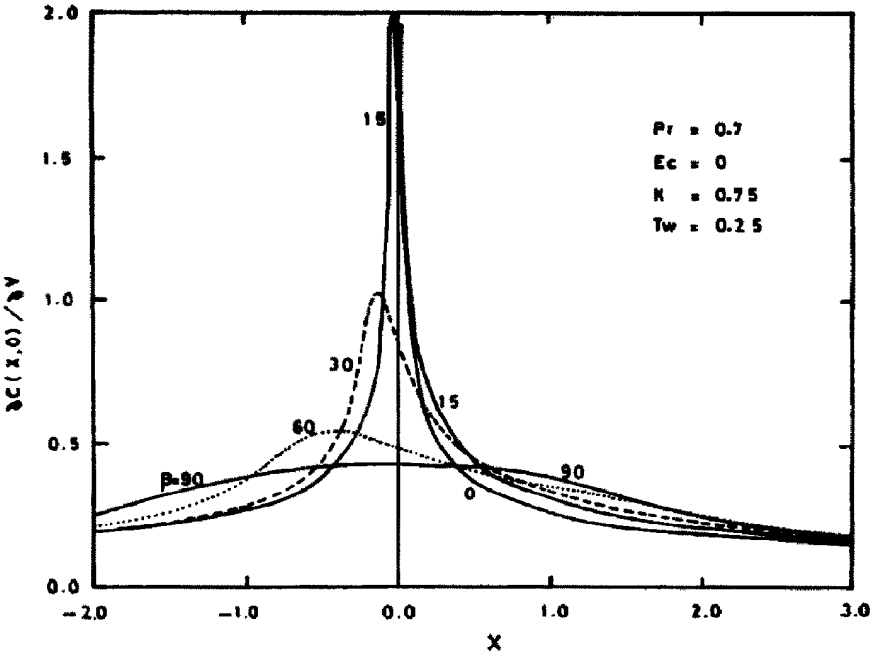

FIG. 7. Concentration gradient at a cold inclined plate ($Pr = 0.7$, $Ec = 0$, $K = 0.75$, $T_w = 0.25$).

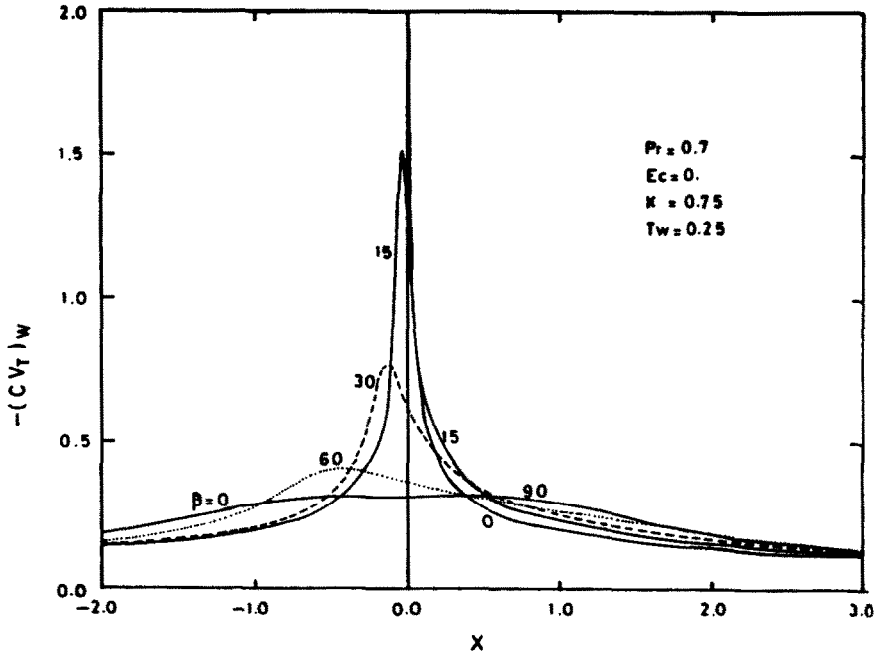

FIG. 8. Particle flux at a cold inclined plate ($Pr = 0.7$, $Ec = 0$, $K = 0.75$, $T_w = 0.25$).

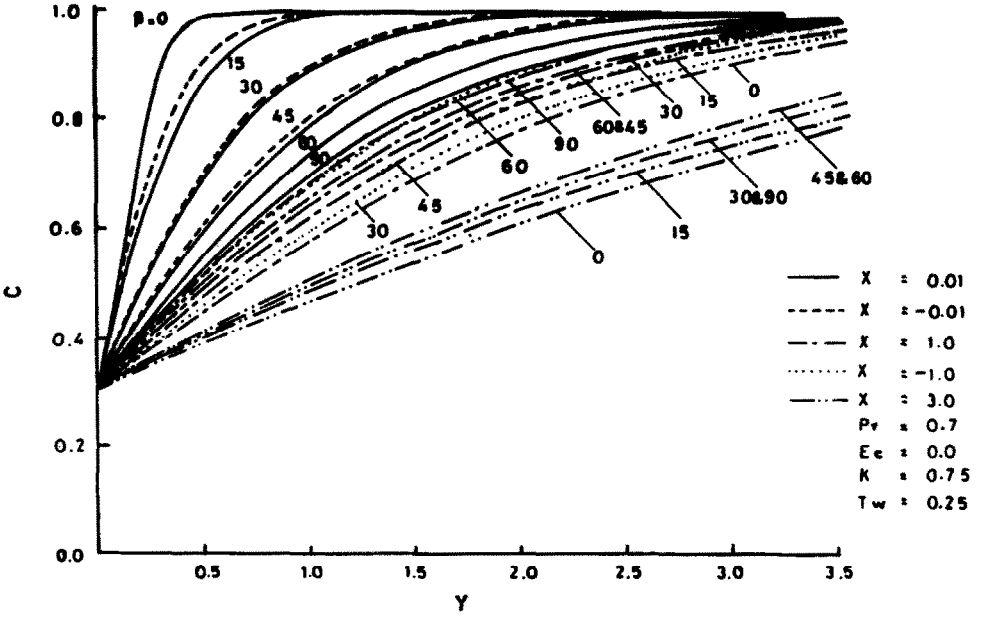

FIG. 9. Particle concentration profiles for a cold inclined plate.

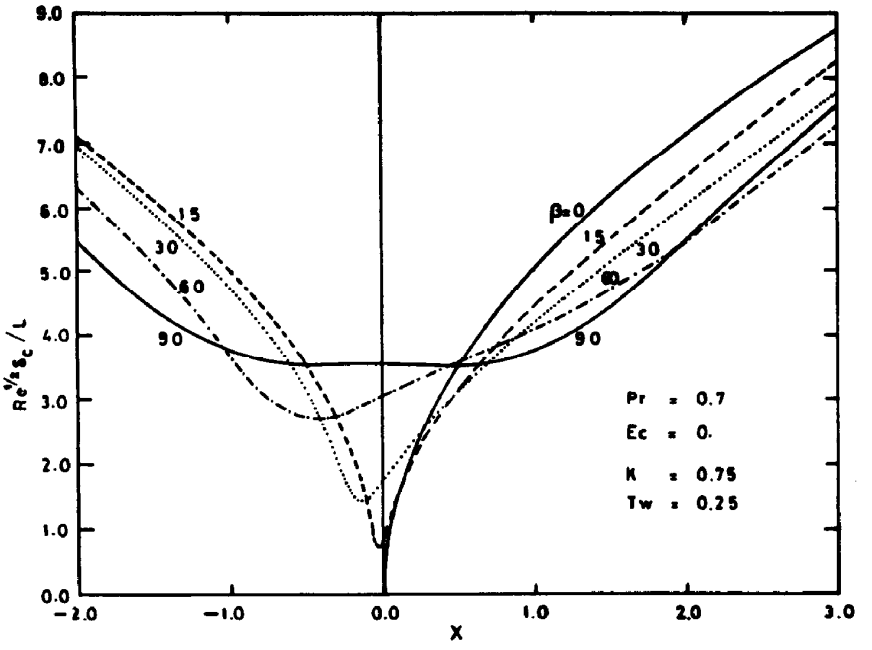

FIG. 10. Concentration boundary layer thickness over a cold inclined plate ($Pr = 0.7$, $Ec = 0$, $K = 0.75$, $T_w = 0.25$).

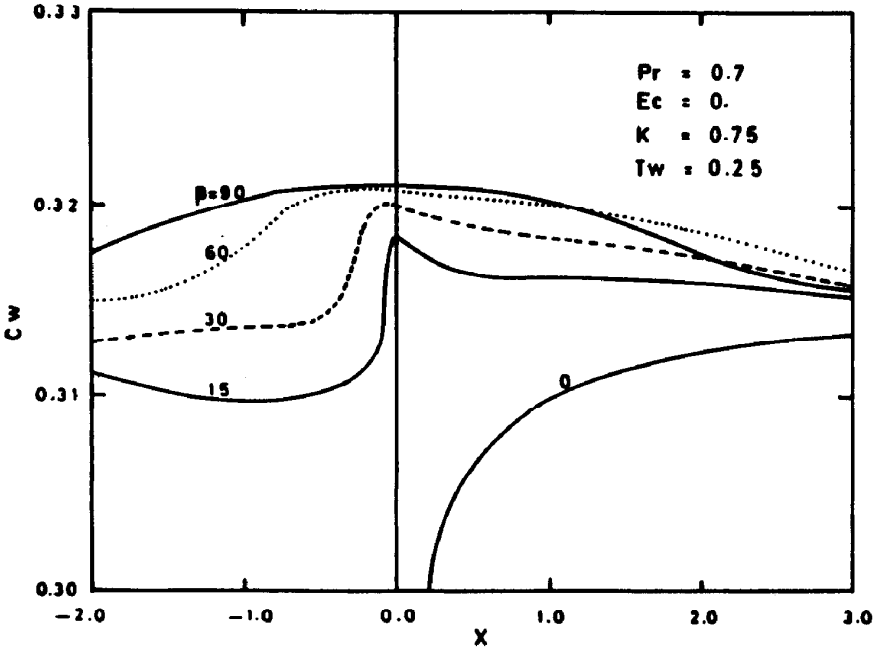

FIG. 11. Particle concentration at a cold inclined plate ($Pr = 0.7$, $Ec = 0$, $K = 0.75$, $T_w = 0.25$).

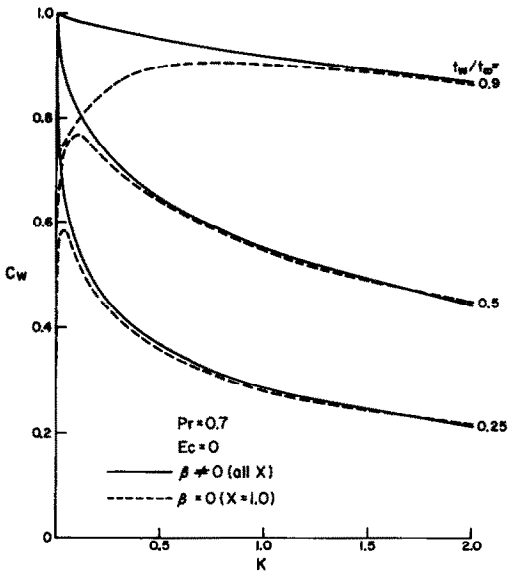

FIG. 12. Variation of concentration at the cold plate with K.

metrical about the Y-axis for $\beta = 90°$. Note that in this as well as in Figs. 3 and 4, we use the boundary layer coordinate Y instead of the physical coordinate y. Thus it may be difficult to visualize that the streamline pattern in Fig. 2 corresponds to $\beta = 15°$.

Figures 3 and 4 show the gas and particle velocity vectors, respectively, in the vicinity of a cold plate inclined at $\beta = 15°$. Clearly, while the gas velocity vectors follow the streamlines of Fig. 2 (note the ratio of ordinate scales on Figs. 2 and 3), the aerosol particles fall to the cold plate in the normal direction due to the thermophoretic velocity component V_T. Recall that while U and V are zero at the plate, V_T is negative at the cold plate. On these figures the length of the velocity vectors is proportional to the magnitude of the velocity at the mid-point of the vector. The ratio of the proportionality constant for the length of the vectors in Fig. 3 to that of the vectors in Fig. 4 is 25. Similar results are obtained at other inclinations of the plate.

4.2. *Thermal characteristics*

Figure 5 shows the dimensionless temperature distribution θ for various angles of impingement at different locations from the stagnation point for $Pr = 0.7$ and $Ec = 0$. There is perfect agreement between the present results and the standard similarity solution at zero incidence [13] denoted by 'stars', thus validating the present results. It may be noted from Fig. 5 that very near the stagnation point, the thermal boundary layer thickness is small for smaller values of β. An opposite situation prevails at $X = 1.0$. A similar behavior is followed by the concentration boundary layer thickness as will be observed in Fig. 10.

Figure 6 shows the local Nusselt number, Nu, based on the slot jet thickness L by the relation

$$Nu = hL/k = -Re^{1/2}(\partial\theta/\partial Y)_w \qquad (16)$$

at different angles of jet impinging on an isothermal plate for $Pr = 0.7$ and $Ec = 0$. The curve for $\beta = 90°$ agrees exactly with that for $H \to \infty$ in Fig. 4 of Miyazaki and Silberman [21]. For $\beta = 90°$, the Nusselt number variation is symmetrical about the stagnation point, and Nu at $X = 0$ is almost twice that at $X = 3$.

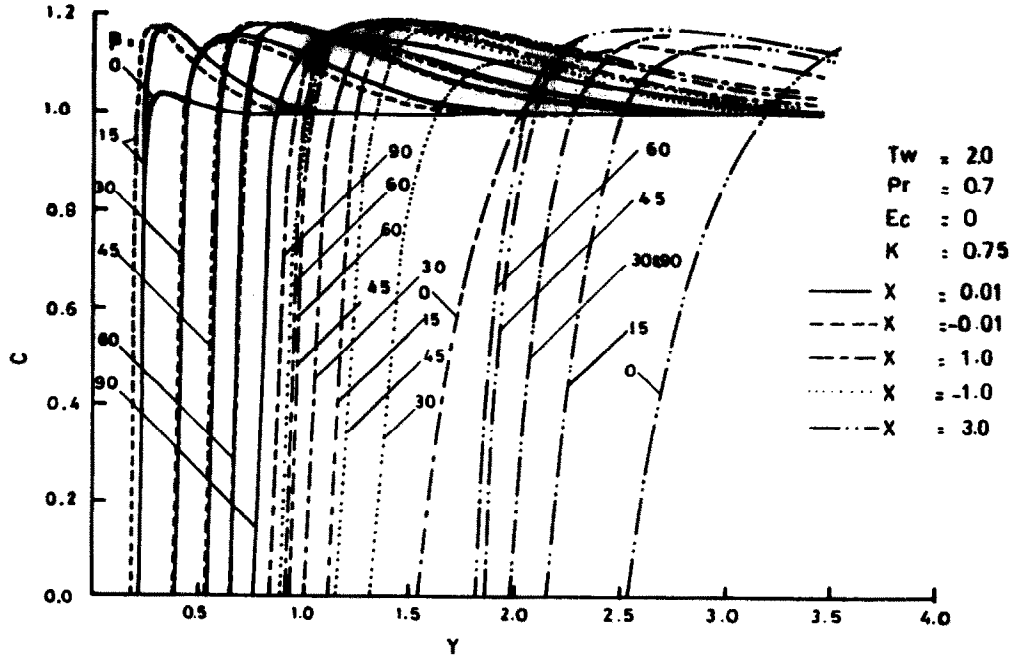

FIG. 13. Particle concentration profiles for a hot inclined plate ($Pr\,K < 1$).

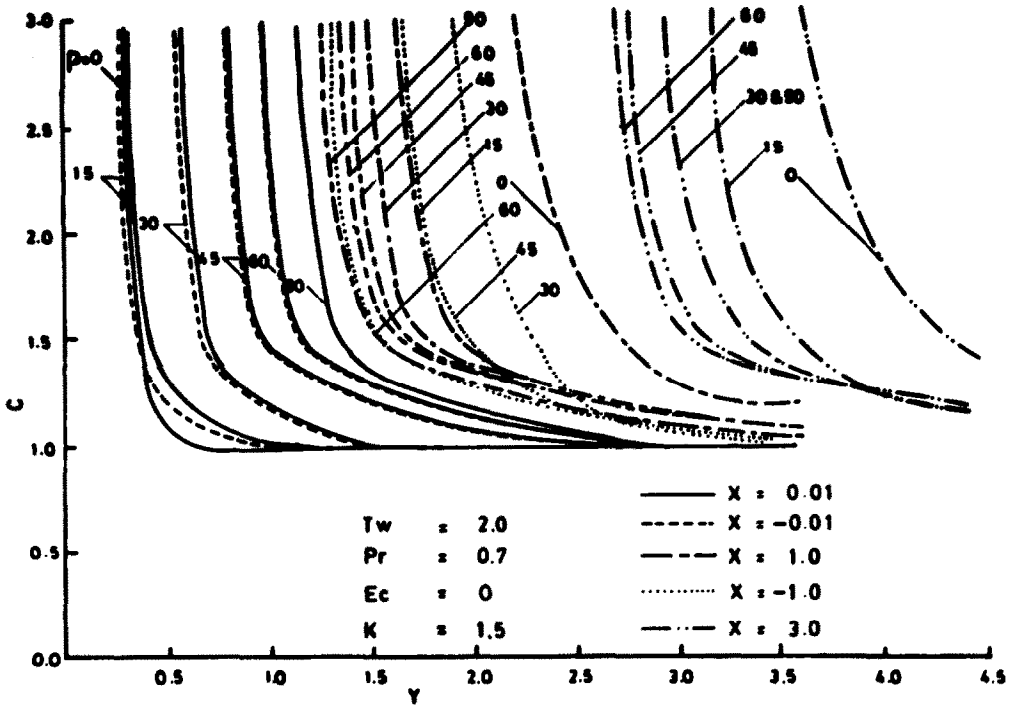

FIG. 14. Particle concentration profiles for a hot inclined plate ($Pr\ K > 1$).

There is a substantial change in the $Nu/Re^{1/2}$ profiles for other values of angle β. The maxima in these profiles lie in the $X < 0$ region, and shift towards the stagnation point as β decreases. At $\beta = 15°$, the maximum value of the local Nusselt number is as much as 10 times that at $X = 3$. It should be noted that the large change in Nusselt numbers with respect to β occurs only in the range $-1 < X < 1$. Outside this range the Nusselt number is very close to that for the flow over a flat plate at zero incidence. The latter is also shown in Fig. 6 based on present computations, and matches perfectly with the exact curve [13] denoted by 'stars'. Similar results are obtained for other Prandtl numbers, and in all cases perfect agreement with the exact results in ref. [13] for $\beta = 0$ and in ref. [21] for $\beta = 90°$ is obtained.

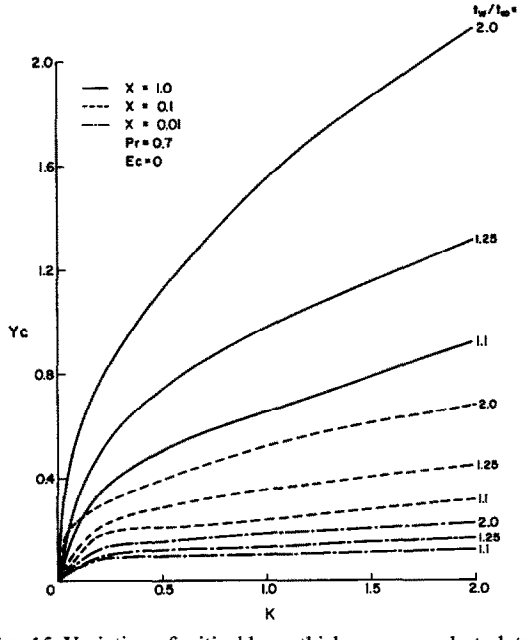

FIG. 15. Variation of critical layer thickness near a hot plate with K for $\beta = 0$.

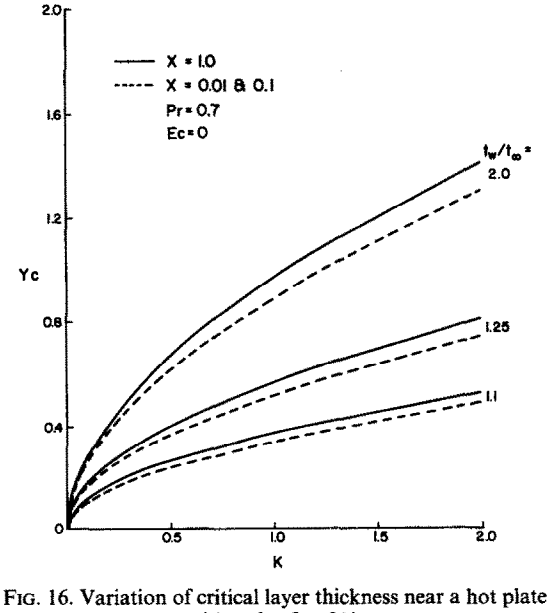

FIG. 16. Variation of critical layer thickness near a hot plate with K for $\beta = 90°$.

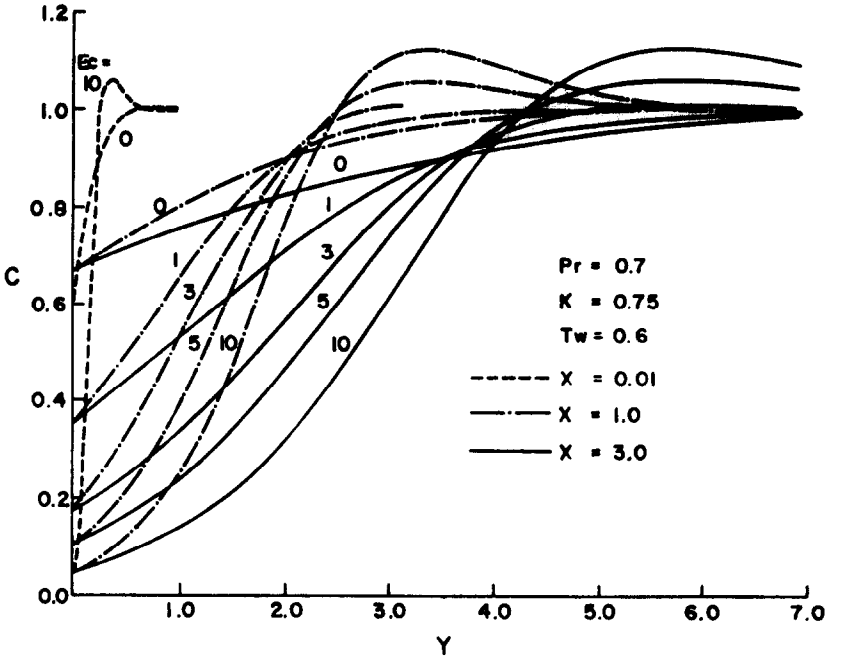

FIG. 17. Effect of Eckert number on concentration profiles over a cold plate at zero angle.

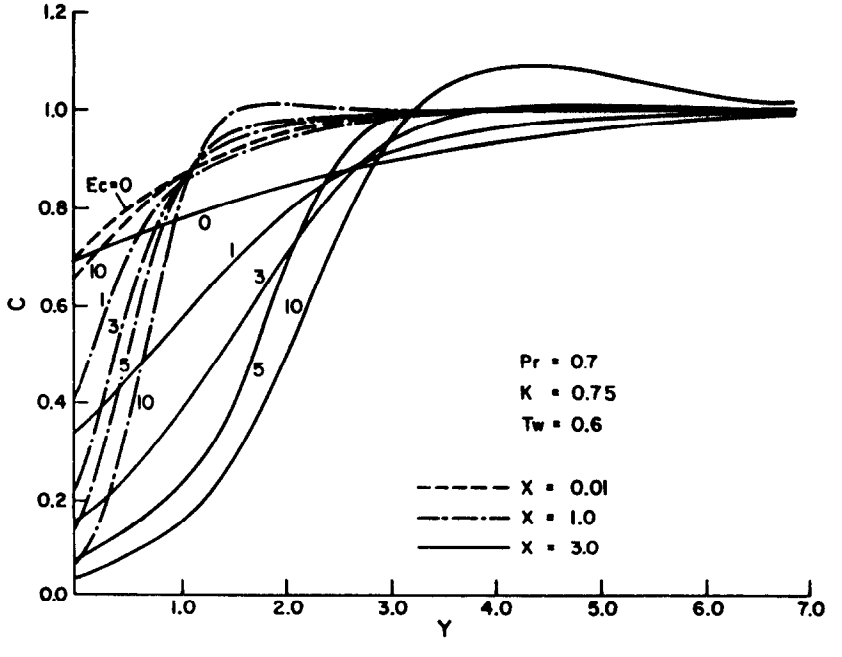

FIG. 18. Effect of Eckert number on concentration profiles over a cold plate at $\beta = 90°$.

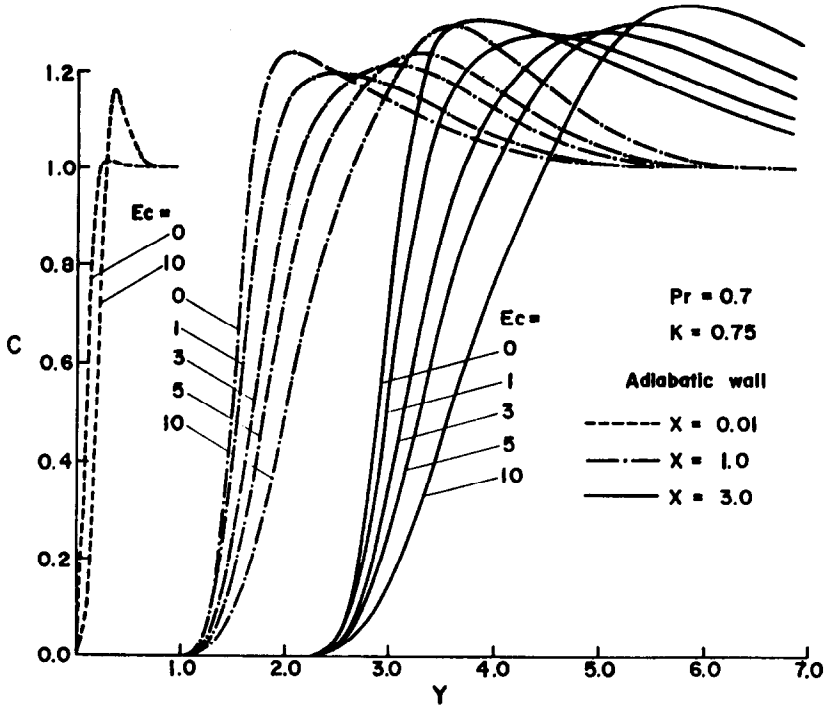

FIG. 19. Effect of Eckert number on concentration profiles over an adiabatic plate at zero angle.

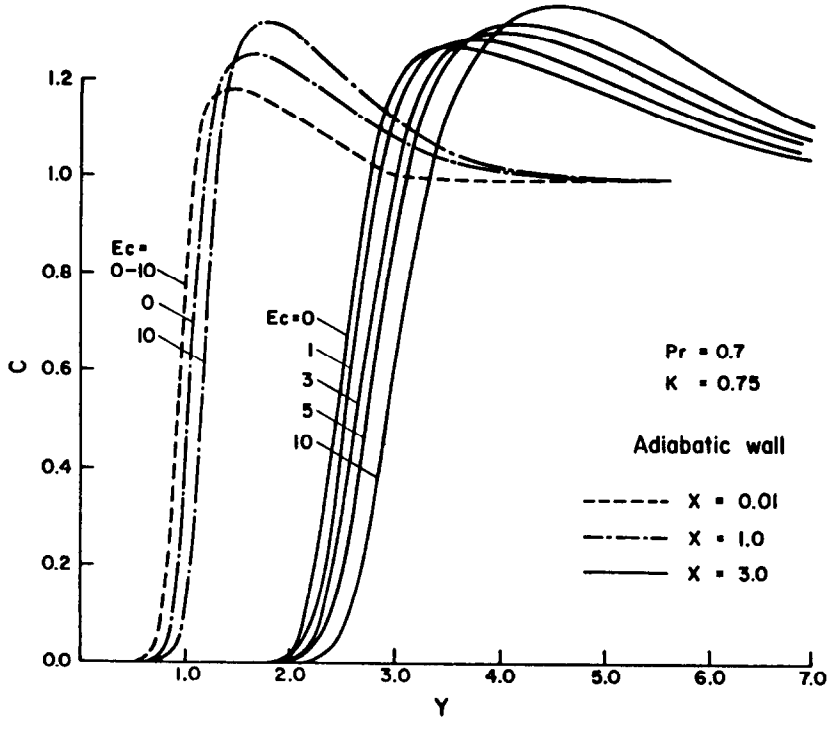

FIG. 20. Effect of Eckert number on concentration profiles over an adiabatic plate at $\beta = 90°$.

4.3. *Results for a cold plate*

Figure 7 shows the local dimensionless concentration gradient, $(\partial C/\partial Y)_w$, at the cold inclined plate for $Pr = 0.7$, $Ec = 0$, $K = 0.75$, and $T_w = 0.25$. These curves are similar to the Nusselt number curves or the normalized temperature gradient curves at the plate in Fig. 6. Very similar curves are obtained for the local dimensionless flux of particles, $J(X)$, given by $-(CV_T)_w$, in Fig. 8 for the cold plate with the same parameter values as in Fig. 7.

In Fig. 9 a number of particle concentration profiles are given for various angles of inclination of the plate, all for $Pr = 0.7$, $Ec = 0$, $K = 0.75$, and $T_w = 0.25$. These profiles are drawn at $X = \pm 0.01, \pm 1.0$ and 3.0, and are very similar to the U-velocity profiles in ref. [14] except that unlike U, $C \neq 0$ at the cold plate. When the results for $\beta = 0$ in Fig. 9 are reduced in terms of the similarity variable of Goren [6], perfect agreement with his results in Fig. 1 is obtained. Similar results are obtained for different values of K and T_w (<1). Figure 10 shows the concentration boundary layer thickness, δ_c, over a cold plate for the same parameters. This thickness is taken as that value of y at which $C = 0.99$. Note that the boundary layer thickness is non-zero at $X = 0$ for $\beta \neq 0$ as expected. Also, for $\beta = 90°$, the boundary layer thickness is almost constant for $|X| \leqslant 0.5$. For other values of β, a minimum value of δ_c is reached in the $X < 0$ region, as expected. The location of this minima shifts away from the stagnation point as β increases, except for $\beta = 90°$. For large values of X, the curves for different β are almost parallel except for $\beta = 90°$. Also, while δ_c gets larger near the stagnation point as β increases, it decreases with β away from the stagnation point except for $\beta = 90°$. These curves for δ_c are similar to those for the hydrodynamic and thermal boundary layer thicknesses in ref. [14].

Figure 11 shows the particle concentration at the cold plate as a function of position along the plate for $Pr = 0.7$, $Ec = 0$, $K = 0.75$, and $T_w = 0.25$. Note that for $\beta \neq 0$, the value of C_w is restricted to a narrow range between 0.31 and 0.32. Similar narrow ranges, with different values, were found for other values of K and T_w (<1). This implies an almost uniform aerosol concentration at any plate angle as long as T_w (<1) and K are constant. Figure 12 shows the effect of K on the cold plate concentration, C_w, for three different plate temperatures in the absence of viscous dissipation. It should be noted that the stagnation point present on the plate for angles of inclination other than zero changes the nature of the curve considerably for small K values. Also, the value of C_w at the cold plate increases as T_w increases but as K decreases.

4.4. *Results for a hot plate*

As explained earlier, there is a critical layer near a hot wall ($T_w > 1$), and the hot wall repels the aerosol particles away from it if $Pr\,K < 1$, thereby forming a particle-free layer near the wall. Figure 13 shows the concentration profiles at different locations on a hot plate for various angles β with $Pr = 0.7$, $Ec = 0$, $K = 0.75$, and $T_w = 2.0$. Particularly striking is the sudden drop to zero of the particle concentration at the critical layer, which is in accord with the observed sharpness of the boundary of the particle-free layer on hot objects. Near the stagnation point ($X = 0.01$) the particle-free layer thickness increases with the angle of inclination but away from the stagnation point ($X = 1.0$) the trend is reversed. Other hot plate temperatures with $Pr\,K < 1$ show similar profiles except for the difference in the maximum concentration attained near the edge of the critical layer with respect to the angle of inclination.

The particle concentration becomes infinite in the critical layer over a hot plate with $Pr\,K > 1$. This fact is seen in Fig. 14 for various angles of inclination of the plate for $Pr = 0.7$, $Ec = 0$, $K = 1.5$, and $T_w = 2.0$. These profiles are drawn at $X = \pm 0.01, \pm 1.0$ and 3.0. The nature of these profiles is similar to that discussed earlier for the profiles in Fig. 13. Near the stagnation point the critical layer thickness increases with β but away from the stagnation point, the trend is reversed.

The effect of thermophoretic coefficient on the critical layer thickness, Y_c, near a hot wall is shown in Figs. 15 and 16 for $\beta = 0$ and 90°, respectively, for $Pr = 0.7$, $Ec = 0$, three different plate temperatures, and at three different locations along the plate. For the maximum angle of impingement ($\beta = 90°$), only a small change is noticed in the profiles as we march along the X-direction (Fig. 16). However, drastic changes occur in similar profiles given in Fig. 15 for the flat plate at zero incidence. The thickness Y_c increases with K as well as with T_w and X.

4.5. *Effect of viscous dissipation*

Figures 17–20 illustrate some of the influences of a finite viscous dissipation rate. Figures 17 and 18 show concentration profiles for $\beta = 0$ and 90°, respectively, for $Pr = 0.7$, $K = 0.75$, $T_w = 0.6$ (cold plate), and for a series of Eckert numbers at three locations along the plate. It is found that Ec has a considerable effect on the concentration profile, specially away from the stagnation point. Particularly striking is the drop in C_w as Ec is raised from 0 to 10. As Ec increases, the particles are blown away from the plate because of the positive value of V_T. Consequently, a significant reduction in particle concentration is noted near the plate along with a corrresponding increase in values greater than unity a little away from the plate. Figures 19 and 20 show the concentration profiles for $\beta = 0$ and 90°, respectively, for a series of Eckert numbers at three locations along an adiabatic plate. Note the relatively small effect of Ec and X on the concentration profiles at $\beta = 90°$ in comparison to that at zero angle of incidence. The general nature of these profiles is

similar to that for flow past a hot plate (Fig. 13) except near the plate where $V_T = 0$ for an adiabatic plate.

5. CONCLUSIONS

The particle concentration boundary layer due to thermophoresis when a slot jet impinges on an inclined plate is studied for a wide range of parameters. Its behavior for the cold plate condition is found to be similar to that of the velocity and thermal boundary layers. The concentration of particles at the cold plate is found to be almost independent of the location along the plate, and of the angle of inclination of the plate. This is interesting since it implies an almost uniform particle concentration at any plate angle as long as the plate temperature (less than the free stream temperature) and thermophoretic coefficient are constant. However, the value of particle concentration at the cold plate increases with the plate temperature. An increase in concentration at the cold plate is also found for a lower thermophoretic coefficient.

For the heated plate condition, the presence of a particle-free layer adjacent to the plate, and particle concentration just outside this layer higher than that in the free stream are notable characteristics of the concentration profiles when the product of Prandtl number and thermophoretic coefficient is less than unity. When this product is greater than unity, a critical layer with very high particle concentration exists adjacent to the plate. The thickness of these layers is a strong function of the angle of jet impingement over the plate as well as of the location along the plate.

Results for the adiabatic plate are very similar to those for the hot plate except that the particle concentration gradient at the plate is zero. The dissipation of mechanical energy in the fluid also has a significant effect on the particle concentration behavior. In particular, it reduces the particle concentration at the cold plate. The simple computational technique using grid adaptation developed here can be used to solve for thermophoresis over any other surface.

Acknowledgements—This work was completed while the first author was on sabbatical at Ohio State University. Use of computing facilities at Ohio State University and helpful comments of the referees are gratefully acknowledged.

REFERENCES

1. H. L. Green and W. R. Lane, *Particulate Clouds: Dusts, Smokes and Mists*, p. 186. Van Nostrand, Princeton, New Jersey (1964).
2. N. A. Fuchs, *The Mechanics of Aerosols*, p. 59. Pergamon Press, New York (1964).
3. K. L. Walker, F. T. Geyling and S. R. Nagel, Thermophoretic deposition of small particles in the Modified Chemical Vapor Deposition (MCVD) process, *J. Am. Ceram. Soc.* **63**, 552–558 (1980).
4. B. V. Derjaguin, A. I. Storozhilova and Ya I. Rabinovich, Experimental verification of the theory of thermophoresis of aerosol particles, *J. Colloid Interface Sci.* **21**, 35–58 (1966).
5. B. V. Derjaguin, Ya I. Rabinovich, A. I. Storozhilova and G. I. Shcherbina, Measurement of the coefficient of thermal slip of gases and the thermophoresis velocity of large size aerosol particles, *J. Colloid Interface Sci.* **57**, 451–461 (1976).
6. S. L. Goren, Thermophoresis of aerosol particles in the laminar boundary layer on a flat plate, *J. Colloid Interface Sci.* **61**, 77–85 (1977).
7. K. L. Walker, G. M. Homsy and F. T. Geyling, Thermophoretic deposition of small particles in laminar tube flow, *J. Colloid Interface Sci.* **69**, 138–147 (1979).
8. M. Epstein, G. M. Hauser and R. E. Henry, Thermophoretic deposition of particles in natural convection flow from a vertical plate, *J. Heat Transfer* **107**, 272–276 (1985).
9. G. M. Homsy, F. T. Geyling and K. L. Walker, Blasius series for thermophoretic deposition of small particles, *J. Colloid Interface Sci.* **83**, 495–501 (1981).
10. T. F. Morse and J. W. Cipolla, Laser modification of thermophoretic deposition, *J. Colloid Interface Sci.* **97**, 137–148 (1984).
11. T. F. Morse, C. Y. Wang and J. W. Cipolla, Laser-induced thermophoresis and particulate deposition efficiency, *J. Heat Transfer* **107**, 155–160 (1985).
12. C. Y. Wang, T. F. Morse and J. W. Cipolla, Laser-induced natural convection and thermophoresis, *J. Heat Transfer* **107**, 161–167 (1985).
13. H. Schlichting, *Boundary Layer Theory*, 7th Edn, Chap. 12. McGraw-Hill, New York (1979).
14. V. K. Garg and S. Jayaraj, Boundary layer analysis for two-dimensional slot jet impingement on inclined plates, *J. Heat Transfer* (1988), in press.
15. J. R. Brock, On the theory of thermal forces acting on aerosol particles, *J. Colloid Sci.* **17**, 768–770 (1962).
16. L. Talbot, R. K. Cheng, R. W. Schefer and D. R. Willis, Thermophoresis of particles in a heated boundary layer, *J. Fluid Mech.* **101**, 737–758 (1980).
17. P. J. Roache, *Computational Fluid Dynamics*, 2nd Edn, Appendix A. Hermosa, Albuquerque (1982).
18. K. Nakahashi and G. S. Deiwert, Three-dimensional adaptive grid method, *AIAA J.* **24**, 948–954 (1986).
19. K. Nakahashi and G. S. Deiwert, Self-adaptive-grid method with application to airfoil flow, *AIAA J.* **25**, 513–520 (1987).
20. R. W. Hornbeck, *Numerical Marching Techniques in Fluid Flows with Heat Transfer*, p. 329. NASA SP-297 (1973).
21. H. Miyazaki and E. Silberman, Flow and heat transfer on a flat plate normal to a two-dimensional laminar jet issuing from a nozzle of finite height, *Int. J. Heat Mass Transfer* **15**, 2097–2107 (1972).

THERMOPHORESE DE PARTICULES D'AEROSOL EN ECOULEMENT LAMINAIRE SUR DES PLAQUES INCLINEES

Résumé—On analyse numériquement le dépôt thermophorétique de petites particules dû à l'impaction d'un jet laminaire rectangulaire sur une plaque inclinée. Les équations de type couche limite sont résolues par une technique de différence finie implicite avec une grille adaptée pour les conditions de plaque froide, chaude ou adiabatique. La concentration de particules sur la plaque froide est à peu près indépendante de la position sur la plaque, et de l'angle d'inclinaison de la plaque tant que la température de la plaque et le coefficient thermophorétique sont constants. Contre la plaque chaude est une couche critique dont l'épaisseur dépend à la fois de la position le long de la plaque et de l'angle d'inclinaison. Selon que cette couche est libre ou pleine de particules, le produit du nombre de Prandtl par le coefficient thermophorétique est inférieur ou supérieur à l'unité. Les résultats pour la plaque adiabatique sont très semblables à ceux de la plaque chaude, sauf pour le gradient de concentration de particules qui est nul sur la plaque. La dissipation de l'énergie mécanique a aussi un effet significatif sur la concentration de particules.

THERMOPHORESE VON AEROSOLPARTIKELN IN LAMINARER STRÖMUNG ÜBER GENEIGTE PLATTEN

Zusammenfassung—Der thermophoretische Abscheidevorgang von kleinen Partikeln beim Auftreffen einer laminaren Schlitzströmung auf eine geneigte Platte wurde numerisch untersucht. Die Grenzschicht-Gleichungen wurden mittels eines implizten Finite-Differenzen-Verfahrens gelöst. Es stellte sich heraus, daß die Partikelkonzentration an einer kalten Platte annähernd unabhängig von der jeweiligen Position an der Platte sowie vom Neigungswinkel ist, solange die Plattentemperatur (sie ist geringer als die Freistromtemperatur) und der thermophoretische Koeffizient konstant sind. Über einer heißen Platte entsteht eine kritische Schicht, deren Dicke sowohl von der Position an der Platte als auch von deren Neigungswinkel abhängt. Ob diese Schicht mit Partikeln besetzt ist oder nicht, hängt von dem Produkt aus Prandtl-Zahl und thermophoretischem Koeffizienten ab, welcher kleiner oder größer als eins sein kann. Die Ergebnisse der Untersuchung an der adiabaten Platte waren denen an der heißen Platte sehr ähnlich, außer der Tatsache, daß der Gradient der Partikelgröße an der Platte null ist. Die Dissipation mechanischer Energie hat ebenfalls einen deutlichen Einfluß auf die Partikelkonzentration.

ТЕРМОФОРЕЗ АЭРОЗОЛЬНЫХ ЧАСТИЦ ПРИ ЛАМИНАРНОМ ТЕЧЕНИИ НАД НАКЛОННЫМИ ПЛАСТИНАМИ

Аннотация—Проводится численный анализ термофоретического осаждения малых частиц при столкновении ламинарной плоской струи с наклонной пластиной. Уравнения пограничного слоя решаются неявным конечноразностным методом с использованием сеточной адаптации для случаев холодных, горячих и адиабатических граничных условий на пластине. Найдено, что концентрация частиц возле холодной пластины почти не зависит от положения точки вдоль пластины и от угла наклона пластины до тех пор, пока температура пластины (величина которой меньше температуы свободного потока) и коэффициент термофореза постоянны. К горячей пластине примыкает критический слой, толщина которого зависит как от координаты вдоль пластины, так и от угла ее наклона. Наличие или отсутствие частиц в слое зависит от того, больше или меньше единицы произведение числа Прандтля на коэффициент термофореза. Результаты, полученные для адиабатической пластины, подобны данным по горячей пластине за исключением того, что градиент концентрации частиц возле пластины равен нулю. Диссипация механической энергии также оказывает существенное влияние на концентрацию частиц.